Turbulent Fluctuation Analysis using Information Geometry in L-H Transitions at KSTAR

M. Parker[1], E. Kim[1,2], M. Choi[3], S. Han[4], J. Juhn[3], KSTAR Team[3]

[1] *Fluid and Complex Systems Research Centre, Coventry University, Coventry, United Kingdom*

[2] *Nuclear Research Institute for Future Technology and Policy, Seoul National University, Seoul, Republic of Korea*

[3] *Korea Institute of Fusion Energy, Daejeon, Republic of Korea*

[4] *Department of Nuclear Engineering, Seoul National University, Seoul, Republic of Korea*

Introduction Predicting H-mode access in future devices like ITER relies on empirical multi-machine scalings that neglect hidden variables and turbulence history [1]. This paper presents an information geometrical analysis of density and temperature fluctuations around L-H transitions from density scan and preemptive edge-localised resonant magnetic perturbations (ERMPs) experiments. Data and initial analysis were presented in [2].

Information geometry is the methods of differential geometry applied to information theory [3, 4, 5], and treats time-dependent probability density functions (PDFs) of variable x as moving trajectories on a statistical Riemannian manifold.

The information length $\mathscr{L}$ traversed by a PDF in finite time interval $[0,t]$ is expressed as:

$$\mathscr{L}(t) = \int_0^t dt' \sqrt{\int dx p(x,t') \left(\frac{\partial \ln p(x,t')}{\partial t'} \right)^2} = \int_0^t dt' \Gamma(t'). \tag{1}$$

$\mathscr{L}$ is a dimensionless metric that quantifies the path-length accrued by the PDF as it evolves in time. It is a measure of the total amount of statistically distinct states passed though during a finite time interval. As shown in Equation 1, it may be expressed as the time-integral of the information rate Γ, where:

$$\Gamma(t) = \sqrt{\int dx p(x,t) \left(\frac{\partial \ln p(x,t)}{\partial t} \right)^2} = \sqrt{\int dx \frac{1}{p(x,t)} \left(\frac{\partial p(x,t)}{\partial t} \right)^2}. \tag{2}$$

The information rate Γ characterises the rate at which new information is revealed during the PDF's evolution.

Experiment, Diagnostics and Empirical Information Geometry Two L-H transition experiments are investigated here: a density scan of three shots using a tungsten divertor and a comparison of two carbon divertor shots where one had preemptive n= 1 Edge-Localised Resonant Magnetic Perturbations (ERMPs) applied. ERMPs are achieved by optimizing 3D control coil geometry to restrict perturbations to the plasma edge region [6]. These experiments used B_T

= 1.9T and I_p = 0.6MA, and the tungsten and carbon divertors had favourable and unfavourable magnetic drifts respectively. An overview of key plasma parameters is shown in Figure 1.

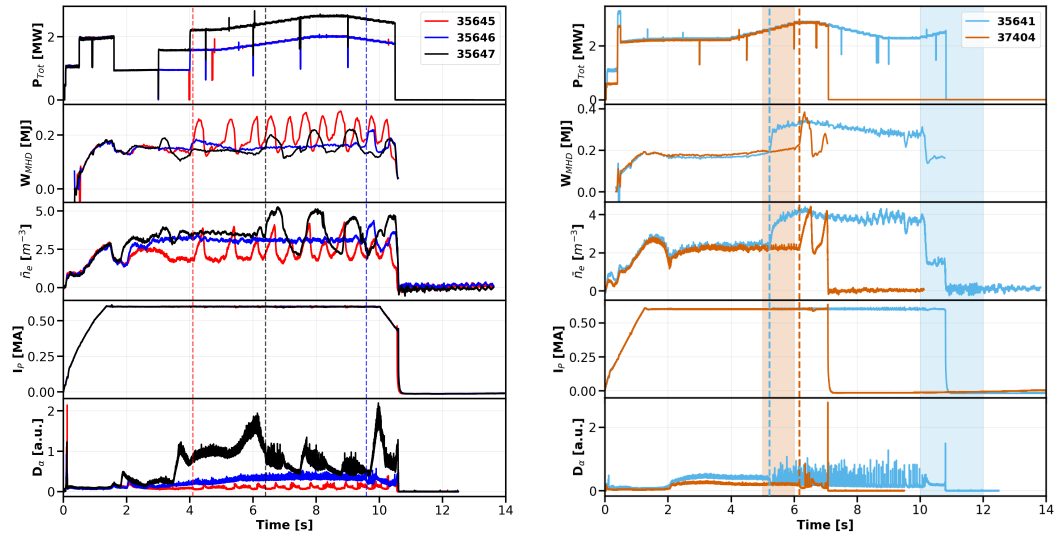

Figure 1: Both columns show, from top to bottom: total NBI power injected, stored MHD energy, line-integrated core electron density, plasma current, and D_α emission. Left: density scan shots 35645/46/47. Right: ERMP shots 35641 and 37404. Dashed lines show the first L-H transition and coloured windows show when ERMPs were applied.

Edge electron density ($\tilde{n}_e$) and temperature ($\tilde{T}_e$) fluctuations were measured with beam emission spectroscopy (BES) and electron cyclotron emission imaging (ECEI). To ensure compatibility, the 1MHz ECEI data was downsampled to match the 0.5MHz BES sampling rate.

To calculate PDFs $p(x,t)$, data are collected into time windows of width $\Delta t = 1$ms and sliding time $dt = 0.5$ms. dt is the difference between successive window centres, meaning they overlap by 0.5ms. PDFs are then calculated by binning these data into normalised histograms, with the number of bins calculated with Rice's rule. To avoid absolute calibration requirements, data are normalized to each window's mean (μ) as $x' = \frac{x}{\mu} - 1$. Background trends are removed via linear detrending within each window, and signals are passed through 65kHz lowpass and 120Hz bandstop filters to reduce stationary machine noise.

Density Scan Figure 2 shows the information geometric quantities of the PDFs for the density scan experiments, along with the D_α emission, core line-averaged density and magneto-spectrograms from an outboard Mirnov Coil measuring $\dot{B}_\theta$. The BES and ECEI channels used took measurements along the midplane at R$\sim$ 2.19m, a few millimetres inboard of the pedestal top. Note that information rate spikes due to beam blips were artificially removed, and information length has been reset to zero at the transition time. In all three shots, for both diagnostics the variance is decreased by the L-H transition, indicating turbulence suppression. L-mode kurtosis fluctuates near $\kappa = 3$ (Gaussian) with frequent spikes indicating intermittency; this intermit-

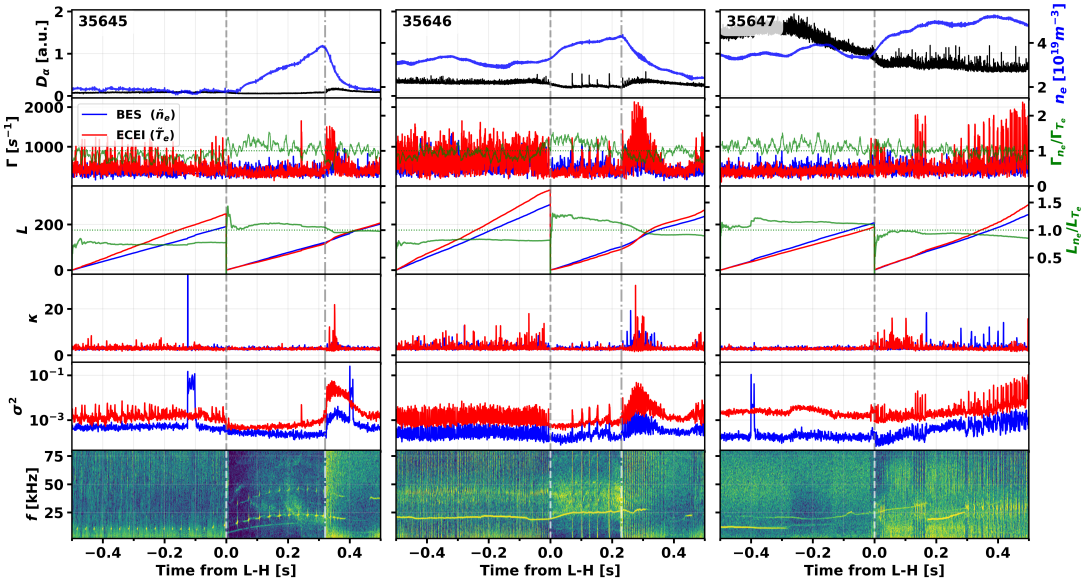

Figure 2: From top to bottom: D_α emission and core line-integrated electron density, information rate, information length, kurtosis of PDFs, variance of PDFs, and outboard Mirnov Coil spectrograms for 35645/46/47 (left to right) using midplane BES and ECEI channels at R$\sim$ 2.19m. Time is shown relative to the first L-H transition and dot-dashed lines show times of H-L transitions.

tency is reduced in H-mode (excepting shot 35647). ELMs are well captured by spikes in both $\tilde{n_e}$ and $\tilde{T_e}$ information rates.

Comparing shots 35645 and 35647 which have approximate line-averaged densities of $1.6 \times 10^{19}\mathrm{m}^{-3}$ and $3.56 \times 10^{19}\mathrm{m}^{-3}$ respectively, the information lengths of $\tilde{n_e}$ and $\tilde{T_e}$ evolve more closely for the high-density shot. This indicates a stronger statistical correlation between the fluctuations. Looking at 35646, despite a similar density to 35647 ($3.17 \times 10^{19}\mathrm{m}^{-3}$) the information lengths are much higher at the transition time and the ratio L_{n_e}/L_{T_e} is closer to that of 35645. This difference in behaviour is caused by the presence of an n=2 coherent magnetic mode at approximately 24kHz.

Preemptive ERMPs Figure 3 shows the same quantities as Figure 2 but for shots 35641 and 37404. Here, the BES and ECEI channels used were along the midplane at R$\sim$ 2.21m. As before, post-transition variance and intermittency drop before ELM onset. While information lengths of $\tilde{n_e}$ at the end of L-mode are similar for both shots, the thermal $\mathscr{L}_{T_e}$ is greater for the preemptive ERMP shot 37404 due to Γ spikes coinciding with chirping features in the magneto-spectrograms. This suggests ERMPs enhance the correlation between magnetic and thermal fluctuations. 0.5s after the transition, the information lengths of 37404 are lower than 35641. This is due to the later onset of less frequent ELMs. While the possibility exists that the difference in ELM behaviour is due to changes in vacuum vessel wall conditions, the similarity in information geometry in L-mode shows that turbulence conditions were similar. This suggests

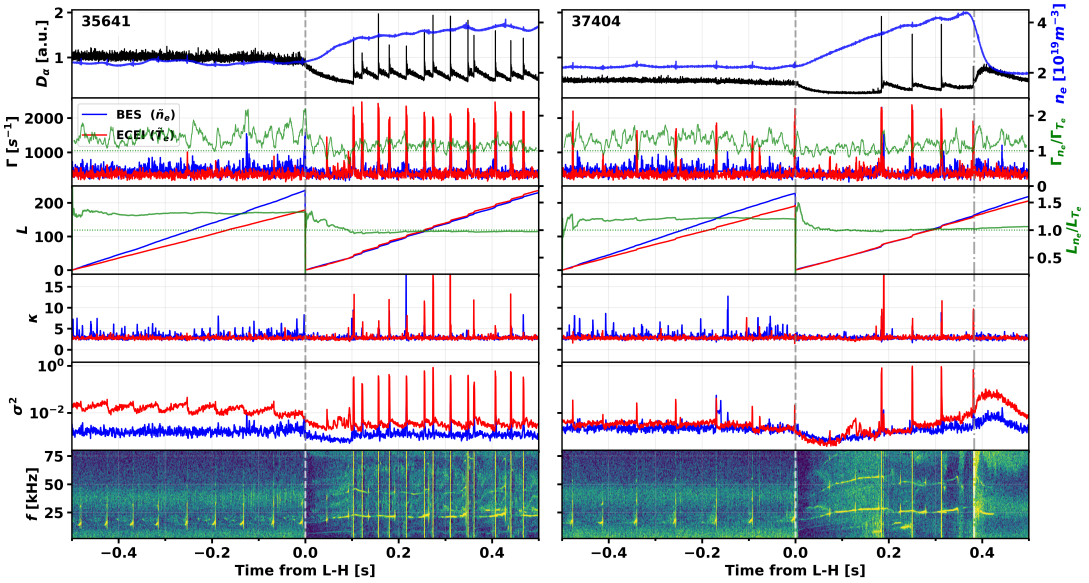

Figure 3: From top to bottom: D_α emission and core line-integrated electron density, information rate, information length, kurtosis of PDFs, variance of PDFs, and outboard Mirnov Coil spectrograms for 35641 (left) and 37404 (right) using midplane BES and ECEI channels at R$\sim$2.21m. Time is shown relative to the first L-H transition and the dot-dashed line shows the time of an H-L transition.

the imprinting of statistical memory by the pre-emptive ERMPs, which were stopped 0.17s before the L-H transition.

Conclusions Information-geometric measures offer a system-agnostic framework to quantify non-equilibrium statistical dynamics and turbulence reorganization around confinement transitions. Unlike standard diagnostics focusing on fluctuation amplitudes, the information rate Γ and path length $\mathscr{L}$ give insight into turbulence's statistical evolution. High-density operation increases $\tilde{n}_e$–$\tilde{T}_e$ statistical correlation, whereas a local $n = 2$ coherent magnetic mode acts as a hidden variable that increases L-mode information lengths and decouples their trajectories. Finally, preemptive ERMPs imprint a statistical memory that alters post-transition ELM onset and frequency. These local, history-dependent dynamics highlight why standard multi-machine scaling laws based on global parameters fail to reliably predict H-mode access.

References

[1] Y. R. Martin, et al. (2008) J. Phys.: Conf. Ser. 123, 012033

[2] E. Kim et al. (2025) Novel Effects of Edge-Localised RMPs and Plasma Density on the L-H Transitions and Transport. Pre-print presented at IAEA FEC 2025, Paper No. EX-P6-3227.

[3] E. Kim (2021) Entropy **23**(11), 1393

[4] T. M. Cover and J. A. Thomas (1991) *Elements of Information Theory*, Wiley-Interscience.

[5] E. Kim and R. Hollerbach (2016) Phys. Rev. E **94**, 052118.

[6] S.M. Yang et al. (2020) Nucl. Fusion **60** 096023

[7] E. Kim, S. Han, M. Parker et al. (2026) Variability of the L–H transition in KSTAR: density dependence and electromagnetic pathways. To be submitted to Plasma Phys. Control. Fusion.